Robotica (2005) volume 23, pp. 51–63. © 2005 Cambridge University Press
DOI: 10.1017/S026357470400092X Printed in the United Kingdom

# Model-based optimal attitude and positioning control of small-scale unmanned helicopter

Jinok Shin, Kenzo Nonami*, Daigo Fujiwara and Kensaku Hazawa

*Dept. of Electronics and Mechanical Engineering, Chiba University, 1-33 Yayoi-cho, Inage-ku, Chiba 263-8522 (Japan)*

(Received in Final Form: June 28, 2004)

## SUMMARY

In this paper, we propose a model-based control system design for autonomous flight and guidance control of a small-scale unmanned helicopter. Small-scale unmanned helicopters have been studied by way of fuzzy and neural network theory, but control that is not based on a model fails to yield good stabilization performance. For this reason, we design a mathematical model and a model-based controller for a small-scale unmanned helicopter system. In order to realize a fully autonomous small-scale unmanned helicopter, we have designed a MIMO attitude controller and a trajectory controller equipped with a Kalman filter-based LQI for a small-scale unmanned helicopter. The design of the trajectory controller takes into consideration the characteristics of attitude closed-loop dynamics. Simulations and experiments have shown that the proposed scheme for attitude control and position control is very useful.

KEYWORDS: Small-scale unmanned helicopter; Model-based MIMO control; Attitude control; Position control; Aero robot.

## 1. INTRODUCTION

Small-scale unmanned helicopters have many applications in dealing with emergency situations; humans cannot come close to a dangerous natural disaster such as an earthquake, flood, an active volcano, or a nuclear disaster.

Among the wide variety of HAVs (unmanned aerial vehicles) that have been developed, small HUAVs (helicopter-based HAVs) have the ability to take off and land vertically as well as the ability to cruise in flight, but the most important capability is hovering. Hovering at a point enables effective observation of the target. Small-scaled HUAVs offer the advantages of low cost and easy operation. Since the development of the first UAVs, research efforts have been focused on military applications. However, nowadays, demand has arisen for UAVs that can be used in handling emergency situations and in industrial applications as an aero-robot.

Unmanned helicopters have been studied with fuzzy[1] or neural network theory,[2,3] but it is not so good performance for unmodel-based control to stabilize it when the system will be changed. Because it will be identified whenever it will be changed.

Small hobby helicopters differ from manned helicopters in rotor head structure and dynamics. Recently, Mettler[4] established the model structure of small helicopters (using a bell-hiller mixing rotor head). Mettler confirmed the validity of the model by a model-based design of PD controller.[5] In our previous studies,[6] we used a method of system identification and designed a SISO controller. However, many parameters are uncertain, including the change of rotor revolution speed and the moment of the fuselage. More importantly, cross-coupling is hard to identify. In many studies, HUAVs are controlled by a SISO (single input single output) controller, but we consider the model as a MIMO (multi input multi output) and design an MIMO controller by LQI (Linear Quadratic Integral). Our research group uses the SF-40, which has the structure of a bell-hiller mixing rotor head.

This paper is organized as follows. In Section 2 we use Mettler's modeling to describe the control concept and the coupled attitude model of SF-40. In Section 3 we design the attitude* feedback gain by LQI and a 2-input 2-output observer-based controller using a Kalman filter. In Section 4 we describe the position dynamics model, which includes a virtual attitude actuator, and design the position controller by LQI. In Section 5 we validate the attitude control and position control through simulations and experimental results in time domain. In the last section we present conclusions about our verified approaches and flight experiments. SF-40 is shown in Figure 1, and the specifications are shown in Table I.

## 2. ATTITUDE MODEL STRUCTURE

First, we describe the concept illustrated in Figure 2. We use a separated feedback system as shown in Figure 2 in order to guarantee flight safety. Even if the hovering feedback system becomes unstable, the input (attitude reference) can be limited by the attitude controller. We limit the pitch and roll angles to $\pm 10$ degrees. That is, the attitude controller prevents the helicopter from falling into a non-linear level. Moreover, separating attitude control from hovering control is effective for optimizing the controller, because control precision depends on attitude control precision.

Figure 3 illustrates the small helicopter coordinates, and Table II shows the state parameters and their physical meanings.

* Corresponding author.

* The term attitude refers to the rotations of the helicopter (pitch, roll and yaw).

Fig. 1. Small-scale unmanned helicopter (SF-40).

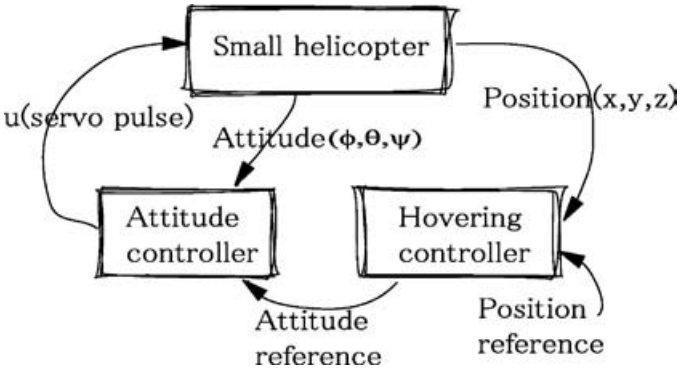


Fig. 2. A concept of small helicopter control.

Table I. Specifications of SF-40 System.

| | |
|---|---|
| Helicopter weight | 9 kgf |
| Engine | 40 cc gasoline engine |
| Main rotor diameter | 1.79 m |
| Length | 1.467 m |
| Sensor system weight | 6 kgf |
| Host computer | 486 DX66Hz |

We adopt Mettler's attitude model, in which pitch and roll are coupled.

Rotor time constants (main rotor tip path plane and stabilizer paddle tip path plane time constants) are very important parameters of a helicopter equipped with a bell-hiller rotor hub system. Another important parameter is the hub tilt spring constant, which influences coupling between the rotor and fuselage.

Table II. Nomenclature.

| Parameter | Definition |
|---|---|
| $p, \phi$ | Roll rate, roll angle of fuselage |
| $q, \theta$ | Pitch rate, pitch angle of fuselage |
| $r, \psi$ | Yaw rate, azimuth angle of fuselage |
| $u, x$ | Longitudinal velocity, Latitude |
| $v, y$ | Lateral velocity, Longitude |
| $w, z$ | Altitude velocity, Altitude |
| $a, b$ | Rotor flapping angle |
| $c, d$ | Stabilizer flapping angle |

The moment of inertia of the rotor blade lock,[7] $\gamma$, is

$$\gamma = \frac{\rho ac(R^4 - r^4)}{I_\beta} \tag{1}$$

The rotor time constant is defined as follows:

$$\tau = \frac{16}{\gamma \Omega} \tag{2}$$

The rotor time constant is defined by the air density $\rho$, the blade chord length $c$, the lift curve slope $a$, the inside radius of rotor $r$, the outside radius of rotor $R$, and the moment of

https://doi.org/10.1017/S026357470400092X Published online by Cambridge University Press

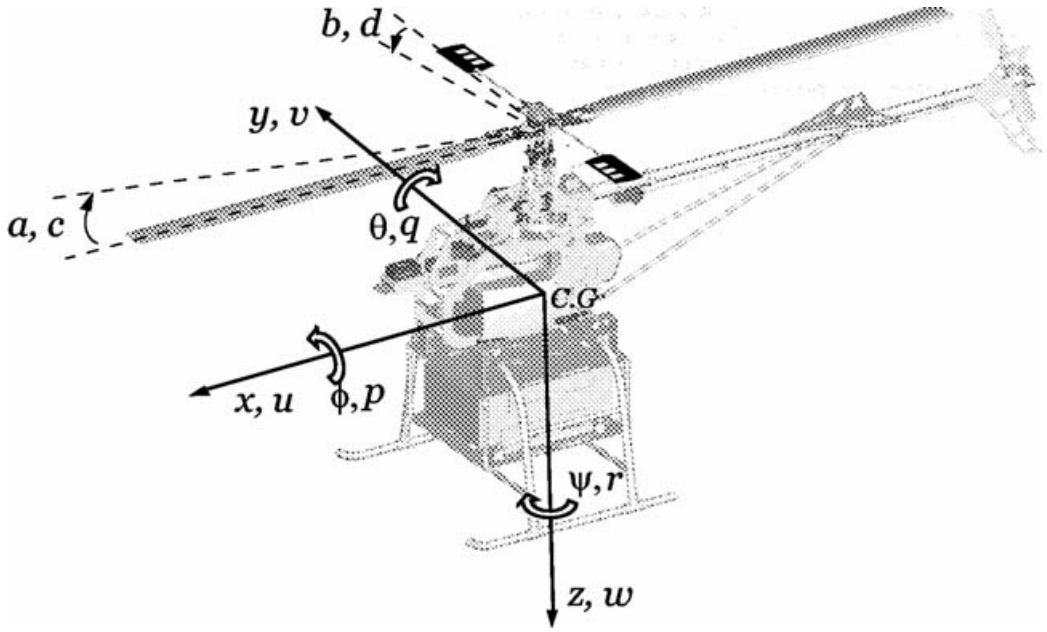


Fig. 3. Helicopter variables with fuselage coordinates.

Table III. Parameters of SF-40.

| | | |
|---|---|---|
| $I_b$ | Moment of inertia of blade (flapping hinge), (kg m$^2$) | 0.0414 |
| $R_b$ | Rotor radius (m) | 0.895 |
| $r_b$ | Rotor inner radius (m) | 0.105 |
| $c_b$ | Blade chord length (m) | 0.06 |
| $a_b$ | Blade lift curve slope (1/rad) | 2.26 |
| $I_s$ | Moment of inertia of paddle with rod (kg m$^2$) | 0.004 |
| $R_s$ | Paddle outside radius (m) | 0.3805 |
| $r_s$ | Paddle inside radius (m) | 0.2675 |
| $c_s$ | Paddle chord length (m) | 0.06 |
| $a_s$ | Paddle lift curve slope (1/rad) | 1.95 |
| $k_\beta$ | Rotor tilt spring constant (Nm/rad) | 38.4 |
| $\rho$ | Air density (kg/m$^3$) | 1.2 |
| $\Omega$ | Rotor revolution speed (rad/s) | 147 |

inertia of the rotor $I_\beta$. $\Omega$ is the constant rotor speed, which is controlled by a governor (engine speed controller). Table III shows the values of the parameters.

The stabilizer's lateral and longitudinal flapping equations are

$$\begin{aligned} \dot{c} &= -\tau_s^{-1}c - q + K_s\tau_s^{-1}\theta_s \\ \dot{d} &= -\tau_s^{-1}d - p + K_s\tau_s^{-1}\phi_s \end{aligned} \tag{3}$$

These are defined in terms of the lateral $d$ and longitudinal $c$ tilt angles of the stabilizer bar plane. $\theta_s$ and $\phi_s$ are the longitudinal and lateral tilt angles of the swash-plate and $K_s$ is the ratio of swash-plate tilt angle to the blade pitch angle of the stabilizer. $\tau_s$ is the stabilizer bar's flapping time constant. The rotor flap equations are as follows:

$$\begin{aligned} \dot{a} &= -\tau_f^{-1}a - q - A'_b b + K_p\tau_f^{-1}c + K_b\tau_f^{-1}\theta_s \\ \dot{b} &= -\tau_f^{-1}b - p + B'_a a + K_p\tau_f^{-1}d + K_b\tau_f^{-1}\phi_s \end{aligned} \tag{4}$$

Table IV. Characteristics of SF-40.

| $K$ | Ratio | Mean |
|---|---|---|
| $K_p$ | 0.6 | Ratio of stabilizer tilt angle to main rotor blade pitch angle |
| $K_s$ | 2.29 | Ratio of swash-plate tilt angle to stabilizer pitch angle |
| $K_b$ | 0.28 | Ratio of swash-plate tilt angle to main rotor blade pitch angle |

Lateral ($b$) and the longitudinal ($a$) tilt angles are defined as tilt angles of the main rotor tip path plane and $K_p$, $K_b$ are the ratio of stabilizer's tilt angle to main rotor blade pitch angle and the ratio of the swash-plate tilt angle to main rotor blade pitch angle, respectively. The gearing of the Bell-Hiller mixing ratio* is $K_b : K_p = 0.28 : 0.6$. $K_s$, $K_p$ and $K_b$ are shown in Table IV. $\tau_f$ is the main rotor blade's flapping time constant. $A'_b$ and $B'_a$ are cross coupling derivatives that influence the rotor's flap and the attitude.

$$A'_b = B'_a = \frac{k_\beta}{2\Omega I_b} \tag{5}$$

$k_\beta$ is the rotor hub tilt spring constant (Nm/rad). Rotor hinge flapping does not occur; the rotor is rigid and rotor tip path plane tilt angle is equal to rotor hub tilt angle.

$$\begin{aligned} L_b &= (hT + k_\beta)/I_{xx} \\ M_a &= (hT + k_\beta)/I_{yy} \end{aligned} \tag{6}$$

* The Bell-Hiller mixing ratio determines the proportion of the main blades cyclic control, i.e. how much comes directly from the swashplate and much comes from the fly bar (stabilizer bar).

https://doi.org/10.1017/S026357470400092X Published online by Cambridge University Press

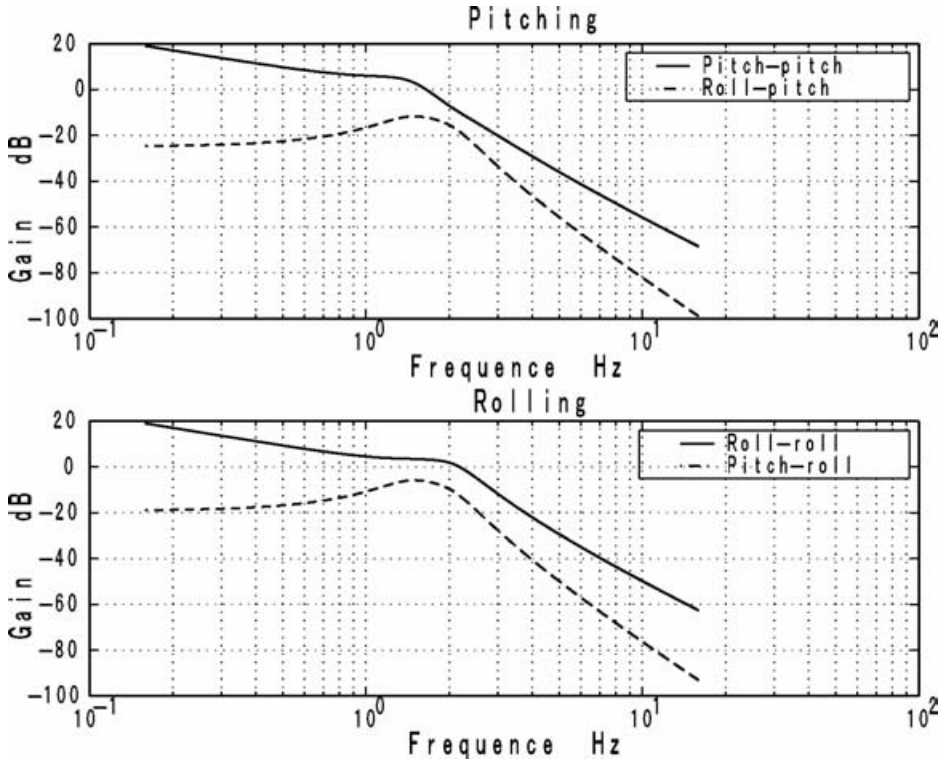


Fig. 4. Bode plots of 2-input 2-output attitude model.

$h$ is the distance between the rotor hub and the c.g. and $T$ is the thrust of main rotor, which in hovering is the same as $mg$. $I_{xx}$ and $I_{yy}$ are the moments of inertia of the fuselage.

The relations between the rotor flapping angle ($a$, $b$) and torque on the fuselage are

$$\begin{aligned} \dot{p} &= L_b b \\ \dot{q} &= M_a a \end{aligned} \tag{7}$$

The parameterized state-space model is shown by Eq. 8.

$$\begin{aligned} \dot{x} &= Ax + Bu \\ y &= Cx \end{aligned}$$

$$A = \begin{bmatrix} -\tau_s^{-1} & 0 & 0 & 0 & -1 & 0 & 0 & 0 \\ 0 & -\tau_s^{-1} & 0 & 0 & 0 & -1 & 0 & 0 \\ K_p\tau_f^{-1} & 0 & -\tau_f^{-1} & -A_b' & -1 & 0 & 0 & 0 \\ 0 & K_p\tau_f^{-1} & B_a' & -\tau_f^{-1} & 0 & -1 & 0 & 0 \\ 0 & 0 & M_a & 0 & 0 & 0 & 0 & 0 \\ 0 & 0 & 0 & L_b & 0 & 0 & 0 & 0 \\ 0 & 0 & 0 & 0 & 1 & 0 & 0 & 0 \\ 0 & 0 & 0 & 0 & 0 & 1 & 0 & 0 \end{bmatrix}$$

$$B = \begin{bmatrix} K_s\tau_s^{-1} & 0 & K_b\tau_f^{-1} & 0 & 0 & 0 & 0 & 0 \\ 0 & K_s\tau_s^{-1} & 0 & K_b\tau_f^{-1} & 0 & 0 & 0 & 0 \end{bmatrix}$$

$$C = \begin{bmatrix} 0 & 0 & 0 & 0 & 0 & 0 & 1 & 0 \\ 0 & 0 & 0 & 0 & 0 & 0 & 0 & 1 \end{bmatrix} \tag{8}$$

The model includes the following states.

$$\begin{aligned} x &= [c\ d\ a\ b\ q\ p\ \theta\ \phi]^T \\ u &= [\theta_s\ \phi_s]^T \end{aligned} \tag{9}$$

Figure 4 shows the frequency response from the swash-plate tilt angle to the attitude angle. Pitching input ($\theta_s$) and rolling input ($\phi_s$) influence each other. Figure 5 shows the impulse input response of the attitude model in time domain. The respective cross-coupling effects are shown.

## 3. ATTITUDE CONTROLLER DESIGN

### *3.1. LQI feedback controller design*

We employed the Linear Quadratic Integral (LQI) theory in designing the attitude controller. The system can be described by

$$\begin{aligned} \dot{x}(t) &= Ax(t) + Bu(t) \\ y(t) &= Cx(t) \end{aligned} \tag{10}$$

The input $u(t)$ is a multi-input consisting of a longitudinal input (elevator) and a lateral input (aileron). $\delta_e$ and $\delta_a$ are the ratios of the pulse width (servo actuator input signal) to the swash-plate tilt angle, respectively.

$$u(t) = [\delta_e\theta_s(t)\ \ \delta_a\phi_s(t)]^T \tag{11}$$

$r$ is the reference consisting of $\theta_r$ and $\phi_r$. The output $y$ is the attitude angles $\theta$ and $\phi$.

$$\begin{aligned} r(t) &= [\theta_r(t)\quad \phi_r(t)]^T, \quad y(t) = [\theta(t)\quad \phi(t)]^T \\ e(t) &= \int_0^t r(t) - y(t)\,dt, \quad \dot{e}(t) = r(t) - y(t) \end{aligned} \tag{12}$$

https://doi.org/10.1017/S026357470400092X Published online by Cambridge University Press

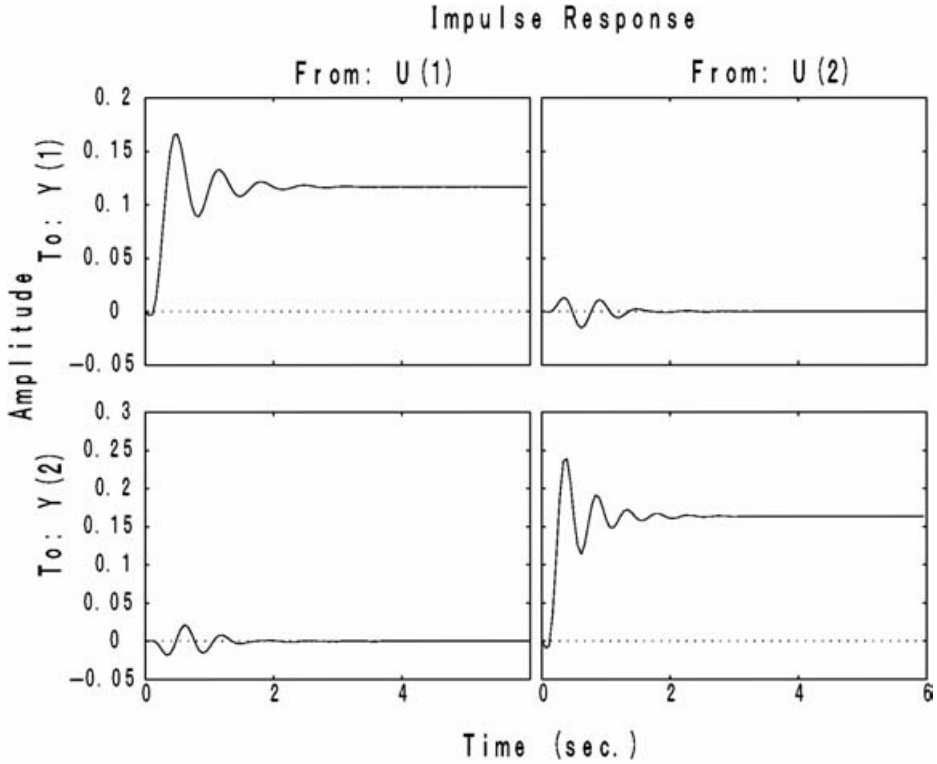


Fig. 5. Impulse response of 2-input 2-output attitude model.

The extended state-space system description involves error ($e(t)$) is described by

$$\frac{d}{dt}\begin{bmatrix} x(t) \\ e(t) \end{bmatrix} = \begin{bmatrix} A & 0 \\ -C & 0 \end{bmatrix}\begin{bmatrix} x(t) \\ e(t) \end{bmatrix} + \begin{bmatrix} B \\ 0 \end{bmatrix} u(t) + \begin{bmatrix} 0 \\ I \end{bmatrix} r(t) \tag{13}$$

The LQR cost function is the sum of the steady-state mean-square weighted state $x_e(t) = [x(t) \quad e(t)]^T$ and the steady-state mean-square weighted actuator signal $u(t)$.

$$J = \int_0^\infty \left[x_e^T(t) Q x_e(t) + u^T(t) R u(t)\right] dt \tag{14}$$

where $Q$ and $R$ are positive semi-definite weight matrices. Standard assumptions are that $(Q, A)$ is observable, $(A, B)$ is controllable, and $R > 0$.

$$F = [F_1 \quad F_2] \tag{15}$$

The feedback gain $F$ is found as the solution of the algebraic Riccati equation, and the optimal feedback control input is shown in the following equation.

$$u(t) = -F x_e(t) = -F_1 x(t) - F_2 e(t) \tag{16}$$

*3.2. Observer design using Kalman filter*

If the system states are not completely accessible, then we design the observer and observer-based controller.

The full-order observer form can be written as

$$\dot{\hat{x}} = A\hat{x} + Bu + K(y - C\hat{x}) \tag{17}$$

where $\hat{x}$ is the optimal estimate of $x$. $K$ is Kalman filter gain:

$$\begin{aligned} K &= \overline{X} + C^T V^{-1} \\ A\overline{X} + \overline{X}A^T - \overline{X}C^T V^{-1} C\overline{X} + GWG^T &= 0 \end{aligned} \tag{18}$$

$\overline{X}$ is the solution of the algebraic Riccati equation. In the design of the Kalman filter, $W$ is power spectrum density of system noise and $V$ is sensor noise. The observer-based controller is described by the state-space realization of the following equations.

$$\frac{d}{dt}\begin{bmatrix} \hat{x}(t) \\ e(t) \end{bmatrix} = \begin{bmatrix} A - BF_1 - KC & -BF_2 \\ 0 & 0 \end{bmatrix}\begin{bmatrix} \hat{x}(t) \\ e(t) \end{bmatrix} + \begin{bmatrix} K & 0 \\ -I & I \end{bmatrix}\begin{bmatrix} y(t) \\ r(t) \end{bmatrix} \tag{19}$$

$$\begin{bmatrix} u(t) \\ e(t) \end{bmatrix} = \begin{bmatrix} -F_1 & -F_2 \\ 0 & 0 \end{bmatrix}\begin{bmatrix} \hat{x}(t) \\ e(t) \end{bmatrix} \tag{20}$$

Figure 6 shows the block diagram of LQI with observer.

## 4. LATERAL AND LONGITUDINAL MODEL

*4.1. Model structure*

The lateral and longitudinal model can be described as

$$\begin{aligned} \dot{u} &= X_u u - g(\theta + a) \\ \dot{v} &= Y_v v + g(\phi + b) \end{aligned} \tag{21}$$

https://doi.org/10.1017/S026357470400092X Published online by Cambridge University Press

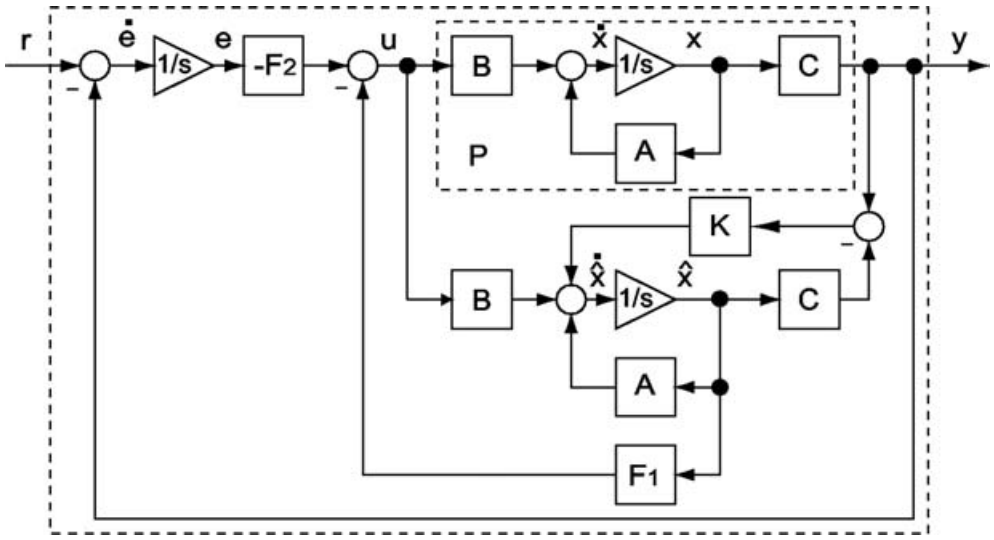


Fig. 6. Block diagram of LQI controller with Kalman filter.

The accelerations of the helicopter's lateral and longitudinal motion depend on the thrust vector. In hovering, thrust is equal to $mg$. If $\theta, a, \phi, b$ are small, then $\sin(\theta + a)$, $\sin(\phi + b)$ terms can be assumed to be linear in hover flight. In this point, we describe the model from input of $\theta_r$, $\phi_r$ to output of longitudinal position ($x$) and lateral position ($y$) including an attitude servo controller (we call this a virtual attitude actuator). The dynamics of the virtual actuator are high-order, but reducing the order is impossible, because if the dynamics of virtual actuator are reduced to low-order, then the rotor flapping states ($a, b$) will be unknown. For this reason, we incorporate the virtual actuator in the system. The following equations are the system matrices of the helicopter's lateral and longitudinal model.

$$\overline{A} = \left[\begin{array}{ccccc|cc} & & (A_e - B_e F)^{10\times 10} & & & 0^{10\times 4} & \\ \hline 0^{2\times 2} & G & 0^{2\times 2} & G & 0^{2\times 2} & V & 0^{2\times 2} \\ \hline & & 0^{2\times 10} & & & I^{2\times 2} & 0^{2\times 2} \end{array}\right]$$

$$\overline{B} = [0^{2\times 8} \quad I^{2\times 2} \quad 0^{2\times 4}]^T$$
$$\overline{C} = [0^{2\times 12} \quad I^{2\times 2}]$$

$$G = \begin{bmatrix} -g & 0 \\ 0 & g \end{bmatrix} \quad I = \begin{bmatrix} 1 & 0 \\ 0 & 1 \end{bmatrix} \quad V = \begin{bmatrix} X_u & 0 \\ 0 & Y_v \end{bmatrix}$$

$$\begin{aligned} \overline{x} &= [c \;\; d \;\; a \;\; b \;\; q \;\; p \;\; \theta \;\; \phi \;\; e_\theta \;\; e_\phi \;\; u \;\; v \;\; x \;\; y]^T \\ \overline{u} &= [\theta_r \;\; \phi_r]^T \end{aligned} \tag{22}$$

$A_e$ and $B_e$ are the extended attitude system matrix in Eq. 13. $F$ is the attitude feedback gain in Eq. 15, and $g$ is gravitational acceleration. $X_u$ and $Y_v$ are speed derivatives. We set $X_u$ and $Y_v$ to zero, when the speed is low. Figure 7 shows bode plots of $G(s)_{x\theta_r}$ and $G(s)_{y\phi_r}$. The plots include notches due to unstable zeros i.e., flapping states ($a$, $b$) and attitude state ($\theta$, $\phi$) cancel the lateral and longitudinal components of the thrust vector, respectively, in the manner of a pendulum. Cancellation of the components of the thrust vector is depicted in Figure 8.

### *4.2. LQI position feedback controller design*

We designed an LQI feedback controller for position control. The system can be described by

$$\dot{\overline{x}}(t) = \overline{A}\overline{x}(t) + \overline{B}\overline{u}(t) \tag{23}$$

The input $\overline{u}(t)$ is a multi-input consisting of $\theta_r$ and $\phi_r$, the references of the attitude actuator.

$$\overline{u}(t) = [\theta_r(t) \;\; \phi_r(t)]^T \tag{24}$$

$\overline{r}$ is the position reference, the output $\overline{y}$ is the $x - y$ position of the helicopter.

$$\begin{aligned} &\overline{r}(t) = [x_r(t) \quad y_r(t)]^T, \quad \overline{y}(t) = [x(t) \quad y(t)]^T \\ &\overline{e}(t) = \int_0^t \overline{r}(t) - \overline{y}(t)\, dt, \quad \dot{\overline{e}}(t) = \overline{r}(t) - \overline{y}(t) \end{aligned} \tag{25}$$

The extended state-space system description involves error ($\overline{e}(t)$) is described by

$$\frac{d}{dt}\begin{bmatrix} \overline{x}(t) \\ \overline{e}(t) \end{bmatrix} = \begin{bmatrix} \overline{A} & 0 \\ -\overline{C} & 0 \end{bmatrix}\begin{bmatrix} \overline{x}(t) \\ \overline{e}(t) \end{bmatrix} + \begin{bmatrix} \overline{B} \\ 0 \end{bmatrix}\overline{u}(t) + \begin{bmatrix} 0 \\ I \end{bmatrix}\overline{r}(t) \tag{26}$$

The LQR cost function is the sum of the steady-state mean-square weighted state $\overline{x}_e(t) = [\,\overline{x}(t) \quad \overline{e}(t)\,]^T$, and the steady-state mean-square weighted attitude actuator reference signals $\overline{u}$.

$$\overline{J} = \int_0^\infty \left[\overline{x}_e^T(t)\overline{Q}\overline{x}_e(t) + \overline{u}^T(t)\overline{R}\overline{u}(t)\right] dt \tag{27}$$

https://doi.org/10.1017/S026357470400092X Published online by Cambridge University Press

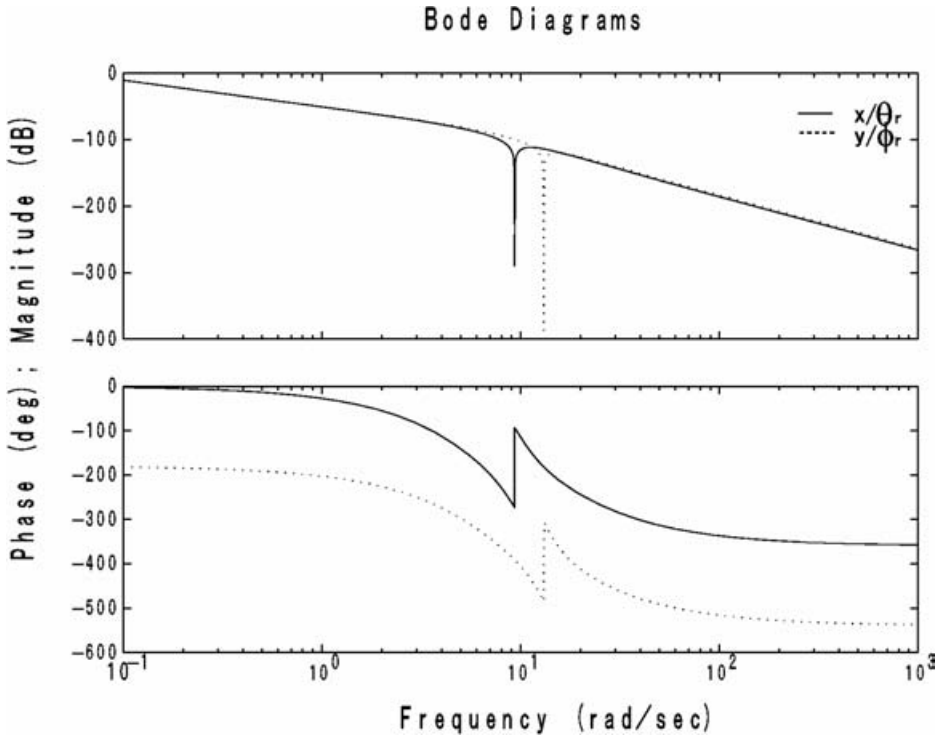


Fig. 7. Bode plots of the lateral and longitudinal motion model (the model is from the attitude reference to the position).

The feedback gain $\overline{F}$ is found as the solution of the algebraic Riccati equation.

The optimal feedback control input is shown in the following equation.

$$\overline{u}(t) = -\overline{F}\overline{x}_e(t) \tag{28}$$

*4.3. Position and velocity observers*

We design different observers for the hovering controller, because embedding a full-order observer is difficult. Therefore, we design an observer that estimates the state of attitude to position.

$$x_p = [u \;\; v \;\; x \;\; y]^T$$
$$u_p = [\theta \;\; \phi]^T$$

$$A_p = \begin{bmatrix} 0 & 0 & X_u & 0 \\ 0 & 0 & 0 & Y_v \\ 1 & 0 & 0 & 0 \\ 0 & 1 & 0 & 0 \end{bmatrix} \quad B_p = \begin{bmatrix} -g & 0 \\ 0 & g \\ 0 & 0 \\ 0 & 0 \end{bmatrix}$$

$$C_p = \begin{bmatrix} 0 & 0 & 1 & 0 \\ 0 & 0 & 0 & 1 \end{bmatrix} \tag{29}$$

$\hat{x}_p$ is the optimal estimate of $x_p$.

$$\dot{\hat{x}}_p = A_p\hat{x}_p + B_p u_p + \overline{K}(\overline{y} - C_p x_p) \tag{30}$$

$\overline{K}$ is the Kalman filter gain. The following equation is the state-space matrix of the velocity-position observer.

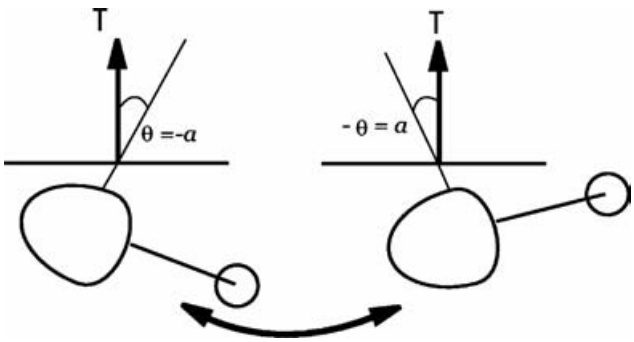


Fig. 8. Cancellation of the components of the longitudinal thrust vector.

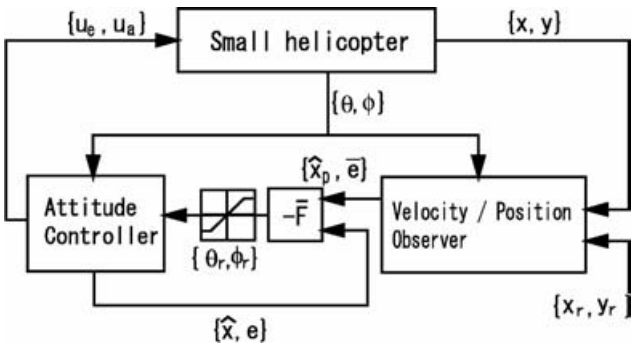


Fig. 9. Control signal flow.

$$\frac{d}{dt}\begin{bmatrix} \hat{x}_p(t) \\ \overline{e}(t) \end{bmatrix} = \begin{bmatrix} A_p - K_p C_p & 0 \\ 0 & 0 \end{bmatrix}\begin{bmatrix} \hat{x}_p(t) \\ \overline{e}(t) \end{bmatrix} + \begin{bmatrix} B_p \\ 0 \end{bmatrix} u_p(t) + \begin{bmatrix} \overline{K} & 0 \\ -I & I \end{bmatrix}\begin{bmatrix} \overline{y}(t) \\ \overline{r}(t) \end{bmatrix} \tag{31}$$

https://doi.org/10.1017/S026357470400092X Published online by Cambridge University Press

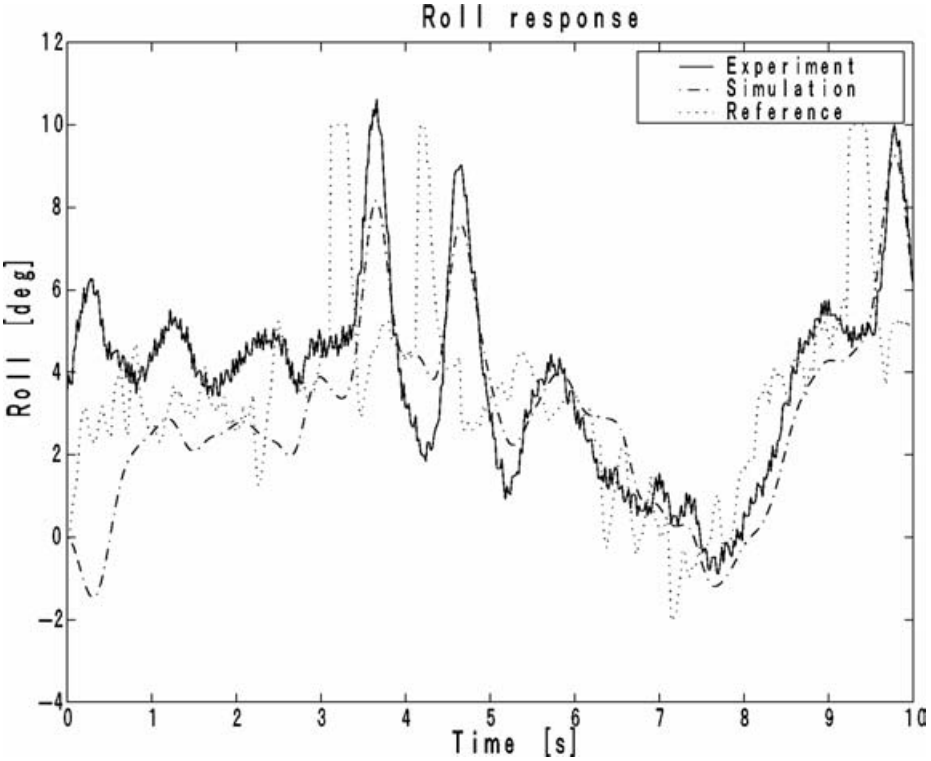


Fig. 10. Comparison of roll control response, experimental and simulation results.

Therefore, the position feedback inputs ($\theta_r$, $\phi_r$) are finally given as follows:

$$\overline{u}(t) = -\overline{F}\,\hat{\overline{x}}_e(t) = -\overline{F}[\hat{x} \quad e \quad \hat{x}_p \quad \overline{e}]^T \qquad (32)$$

$\hat{x}$ and $e$ are state estimation and error in Eq. 19. Figure 9 shows a flowchart of the control signal.

## 5. FLIGHT EXPERIMENTS AND SIMULATION RESULTS

Flight experiments were carried out without heave control. An operator controlled the heave manually. The azimuth was controlled by the LQI controller described in our previous work. This controller maintains the heading of the

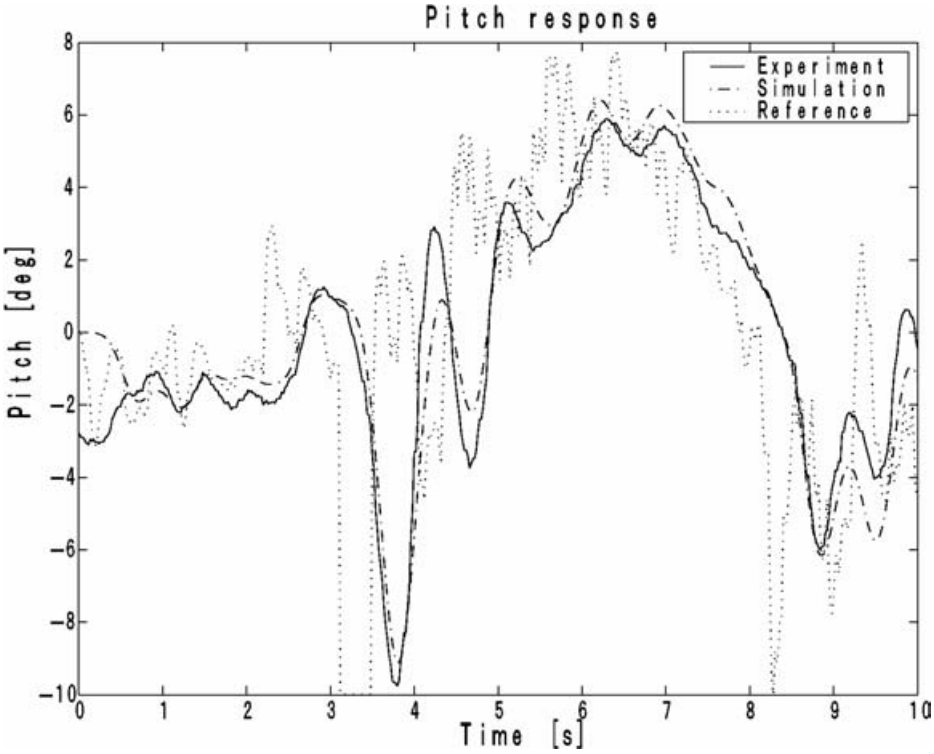


Fig. 11. Comparison of pitch control response, experimental and simulation results.

https://doi.org/10.1017/S026357470400092X Published online by Cambridge University Press

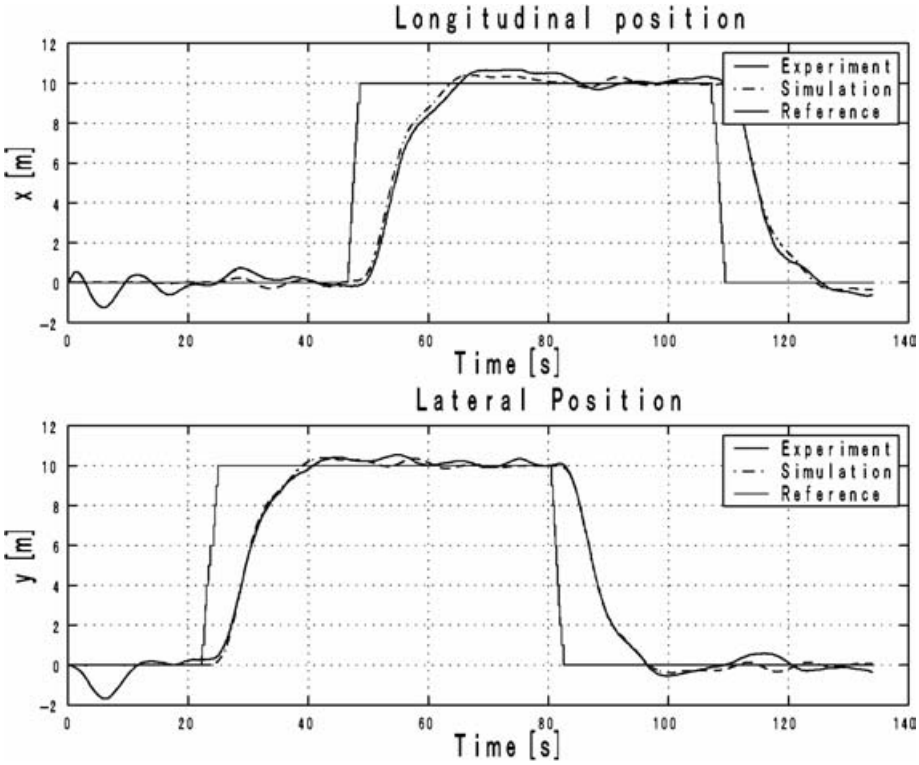


Fig. 12. Position control results of x and y in time domain.

helicopter toward the north. We used a position sensor RT-2 (RTK DGPS, Novatel) and an attitude sensor (a commercial product). Figures 10 and 11 compare the results of the attitude control response simulation with the experimental results in time domain. The comparisons shows that the LQI feedback system is available and the attitudes are well limited to $\pm 10$ degrees. Figure 12 presents the position control results of $x$ and $y$ in time domain, respectively.

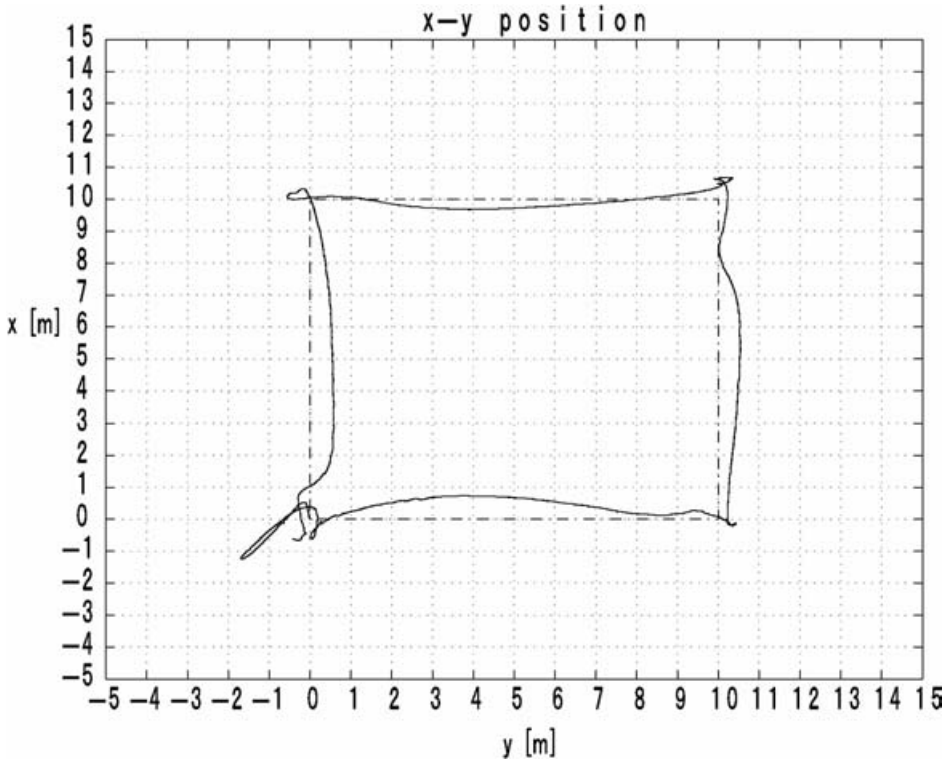


Fig. 13. Flight trajectory result in x – y coordinates.

https://doi.org/10.1017/S026357470400092X Published online by Cambridge University Press

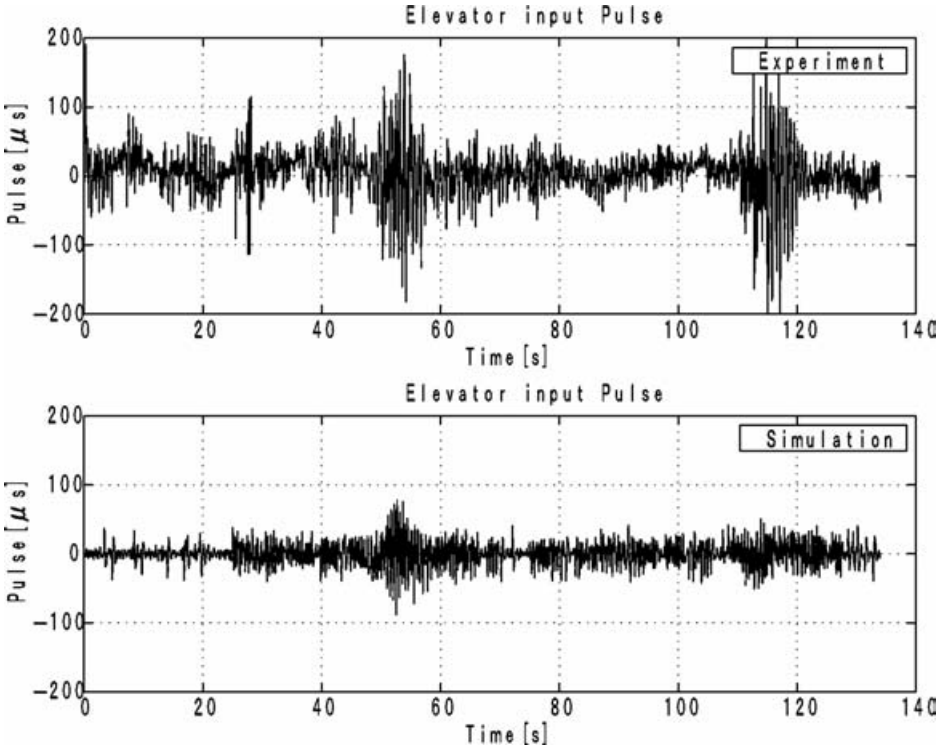


Fig. 14. Elevator input pulse width in flight experiment and simulation.

Figure 13 presents the flight trajectory result of figure 12 in $x-y$ dimensions. Figure 14 and 15 show the elevator input and the aileron input pulse width in the flight experiments and the simulation. Figure 16 and 17 compare experimental results of the pitch and roll angle with simulation results. Figure 18 and 19 compare experiments results of the attitude reference with simulation results in time domain.

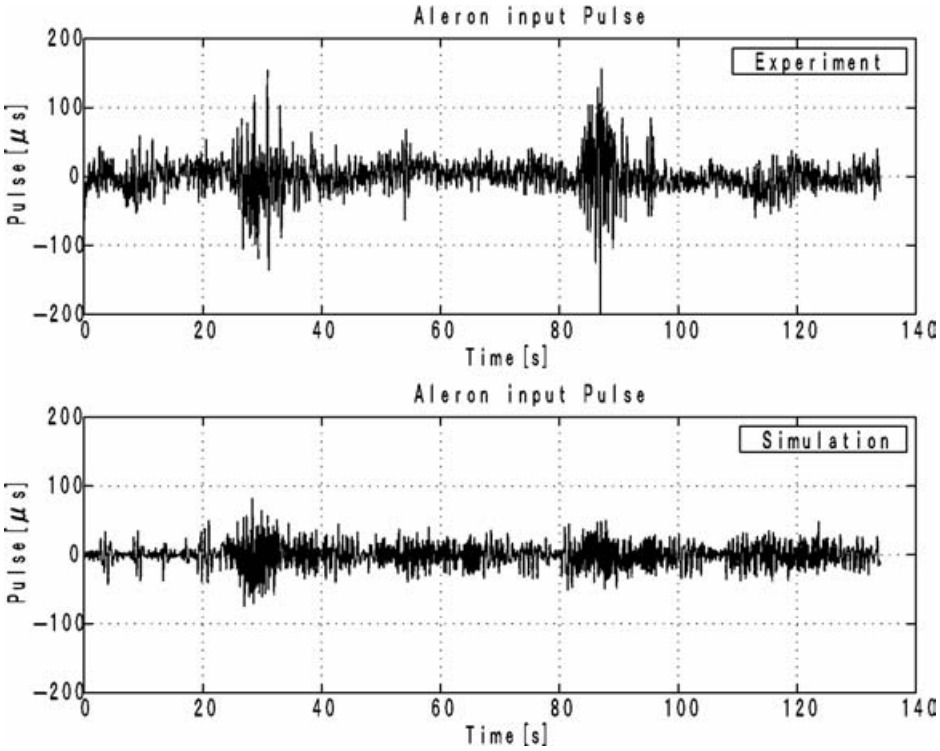


Fig. 15. Aileron input pulse width in flight experiment and simulation.

https://doi.org/10.1017/S026357470400092X Published online by Cambridge University Press

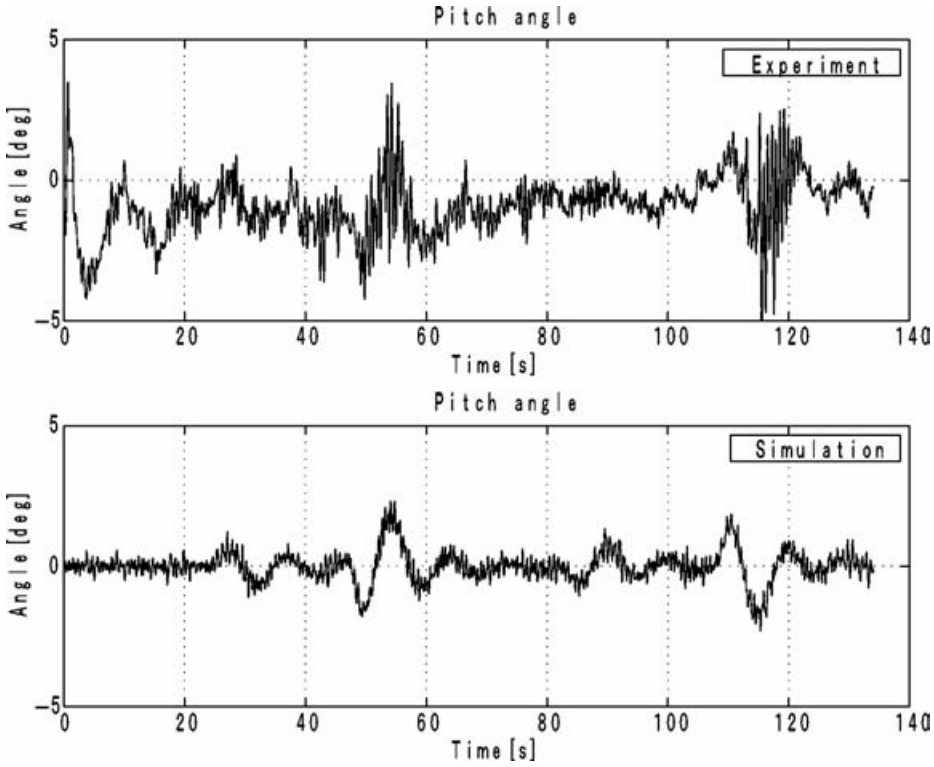


Fig. 16. Comparison of pitch angle response, experimental and simulation results (pitch angle response of the reference as a feedback input of the position controller).

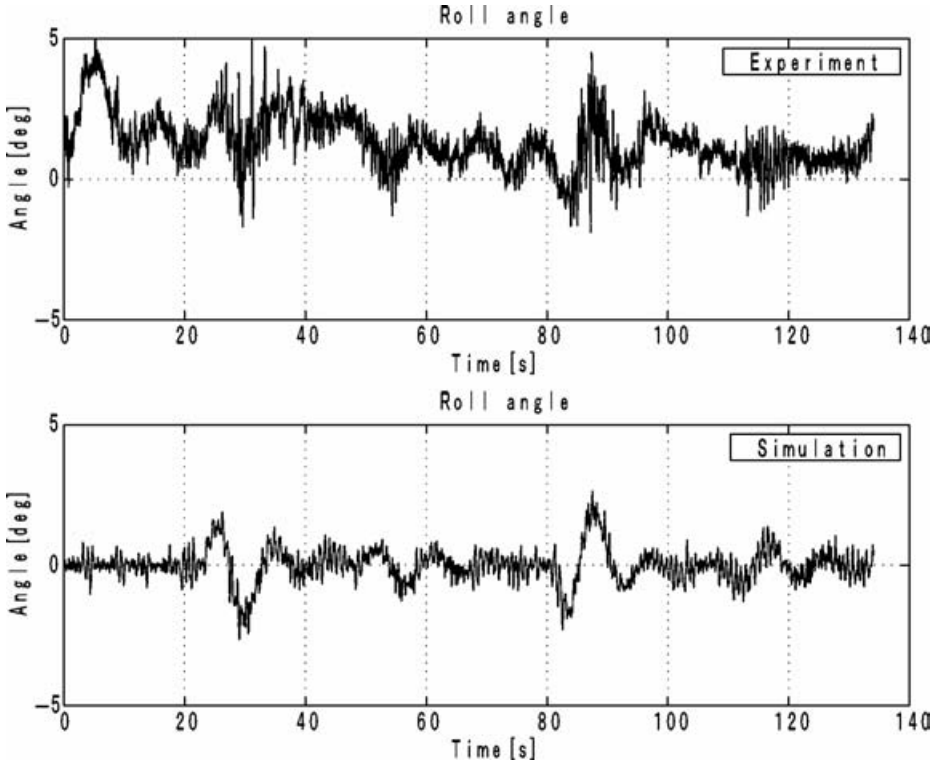


Fig. 17. Comparison of roll angle response, experimental and simulation results (roll angle response of the reference as a feedback input of the position controller).

https://doi.org/10.1017/S026357470400092X Published online by Cambridge University Press

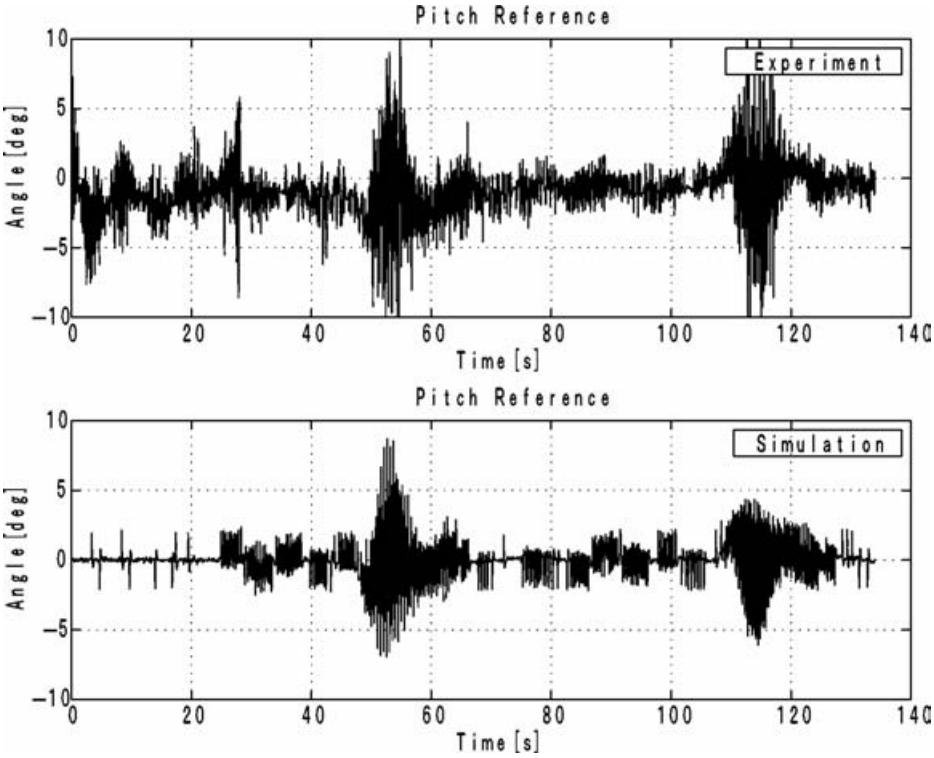


Fig. 18. Comparison of pitch angle reference, experimental and simulation results (feedback input of the position controller).

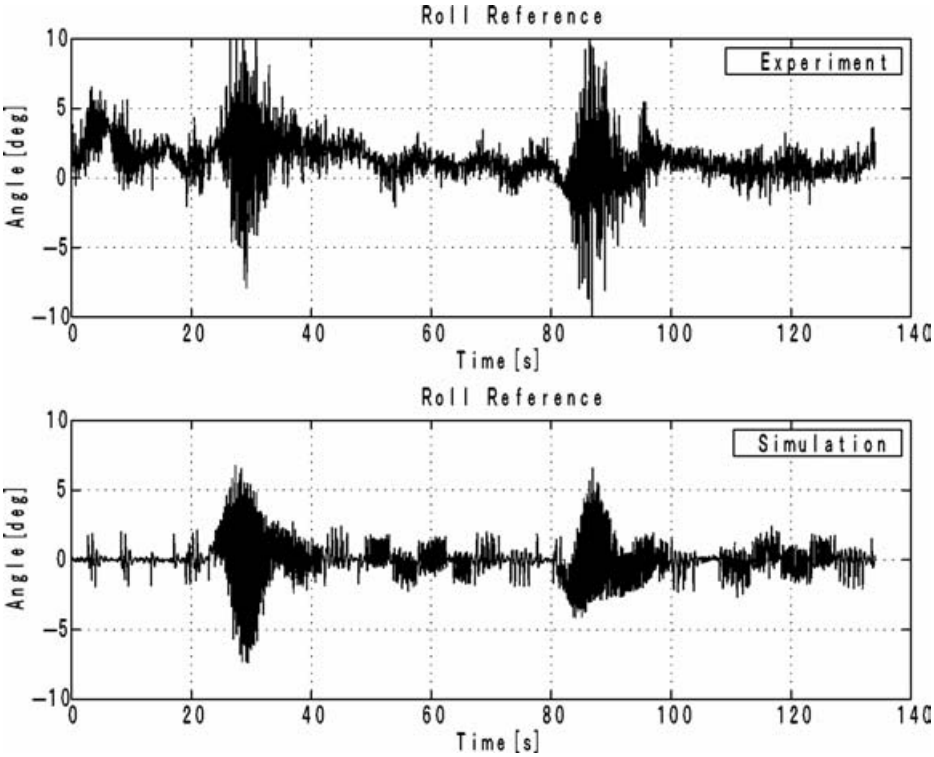


Fig. 19. Comparison of roll angle reference, experimental and simulation results (feedback input of the position controller).

## 6. CONCLUSIONS

We designed a MIMO attitude controller for a small-scale unmanned helicopter and successfully controlled the helicopter's attitude. The performance of the attitude controller was validated by simulation and experimental data in the time domain.

The virtual attitude actuator has been considered in flight dynamics and provides flight safety. The limiting of attitude effectively maintains the helicopter out of the nonlinear region. We also designed a MIMO position controller and successfully achieved hovering and reference flight.

https://doi.org/10.1017/S026357470400092X Published online by Cambridge University Press

## References


1. Hung T. Nguyen and Nadipuram R. Prasad, "Development of an Intelligent Unmanned Helicopter," **In**: *Fuzzy Modeling and Control: Selected Works of M. Sugeno* (CRC press, NewYork, US, 1999) pp. 13–43.
2. J. V. R. Prasad, A. J. Calise, Y. Pei and J. E. Corban, "Adaptive Nonlinear Controller Synthesis and Flight Test Evaluation on an Unmanned Helicopter," *IEEE, International Conference on Control Applications* (1999) pp. 137–142 .
3. Anthony J. Calsie and Rolf T. Rysdk, "Nonlinear Adaptive Flight Control Using Neural Networks," *IEEE Controls Systems Magazine* **18**, No. 6, 14–25 (1998).
4. Bernard Mettler, *Identification Modeling and Characteristics of Miniature Rotorcraft* (Kluwer Academic, Massachusetts, 2003) pp. 53–92.
5. B. Mettler, M. B. Tischler and T. Kanade, "Attitude Control Optimization for a Small-Scale Unmanned Helicopter", *AIAA Guidance, Navigation and Control Conference* (2000) pp. 40–59.
6. J. Shin, D. Fujiwara, K. Hazawa and K. Nonami, "Attitude Control and Hovering Control of Radio-Controlled Helicopter," *Transaction of the Japan Society of Mechanical Engineers, Series C* **68**, 148–155 (2002).
7. George Done and David Balmford, *Bramwell's Helicopter Dynamics*, 2nd ed. (Butterworth Heinemann, Oxford, UK, 2001).


https://doi.org/10.1017/S026357470400092X Published online by Cambridge University Press